Catalysis Today 138 (2008) 210–215

Contents lists available at ScienceDirect

Catalysis Today

journal homepage: www.elsevier.com/locate/cattod

Gold supported on mesoporous titania thin films for application in microstructured reactors in low-temperature water-gas shift reaction

Evgeny V. Rebrov [a,*], Angel Berenguer-Murcia [b], Brian F.G. Johnson [b], Jaap C. Schouten [a]

[a] Department of Chemical Engineering and Chemistry, Eindhoven University of Technology, P.O. Box 513, 5600 MB Eindhoven, The Netherlands
[b] Department of Chemistry, Cambridge University, Lensfield Road, CB2 1EW Cambridge, UK

ARTICLE INFO

Article history:
Available online 20 August 2008

Keywords:
Gold nanoparticles
Mesoporous titania
Water-gas shift
Microstructured reactor

ABSTRACT

Au (1 wt.%)/TiO_2 catalytic thin films were prepared on a surface-modified titanium substrate for application in a water-gas shift (WGS) microstructured reactor. Au-containing mesoporous titania films were synthesized using Pluronic 127 surfactant as a structure directing agent and titanium tetrabutoxide as titania source. Colloidal gold nanoparticles of 4 nm diameter were added to the synthesis sol prior to spin-coating. The resulting thin films were characterized by X-ray diffraction, transmission electron microscopy, ethanol adsorption–desorption isotherms and spectroscopic ellipsometry. Catalytic activity and selectivity were measured for the WGS reaction at temperatures between 220 and 290 °C. The reaction rate measured at CO conversions of below 10% was similar to that reported for gold supported on mesoporous titania and on ceria modified mesoporous titania pelletized catalysts prepared via deposition–precipitation.

1. Introduction

For portable and transport applications, the most convenient and economical way of producing hydrogen is through the on-board reforming of hydrocarbon fuels in a fuel processor (FP) that is combined with a fuel cell (FC) to form an integrated power supply device [1–3]. Portable fossil fuel reforming by means of catalytic processes [4] is currently the most widely used method for hydrogen production and this will continue until hydrogen production using renewable energies becomes economically feasible. In the reforming of gasoline or natural gas, a hydrogen-rich gas is produced with a carbon monoxide concentration of 8–12 vol.%. Since CO is a poison for proton exchange membrane FC catalysts, the water-gas shift (WGS) reaction is used to reduce its concentration to levels below 1 vol.%, thereby increasing the H_2 yield. A viable WGS catalyst for an automotive fuel processor should demonstrate sufficient activity over a reasonable temperature window, be stable for more than 5000 h, be non-pyrophoric (a feature not possessed by conventional Cu-based WGS catalysts), and should not require a lengthy in situ pre-reduction procedure. Optimization of the size and efficiency of the fuel processor is one of the technological hurdles that must be overcome. Over the last decade, microreaction technology has gained increasing importance in fuel processing since the size reduction in reactor dimensions allows the significant enhancement of heat and mass transfer rates [1,4,5]. Microchannel reactors work under laminar flow conditions creating a low-pressure drop compared to randomly packed fixed bed reactors. Usually, the geometric surface area of the microchannels is insufficient for the performance of catalytic reactions. The efficient use of microstructured catalytic reactors requires a shaping of the catalyst, and this is usually achieved by the deposition of thin catalytic coatings on the walls of the reactor channels to increase the surface area. In this case, a WGS microstructured reactor for a fuel processor can approach sizes of up to an order of magnitude smaller than that of a conventional fixed bed reactor.

Inorganic mesoporous thin films have attracted considerable attention because of their large surface areas and narrow pore size distributions. These make them attractive candidates as catalyst supports [6,7]. Gold supported on mesoporous titania and zirconia have already been reported to be promising supports for catalysts in the WGS reaction [8–13]. The catalytic activity, and especially the stability, of gold catalysts strongly depends on both the state and structure of the support and on the specific interactions between gold and support [12,14,15]. In this study, we have applied a different approach, in which colloidal Au nanoparticles of ca. 4 nm diameter were introduced to a titania sol during hydrolysis of the inorganic precursor. Sol deposition was carried

* Corresponding author. Tel.: +31 40 2475548; fax: +31 40 2446653.
E-mail address: e.rebrov@tue.nl (E.V. Rebrov).

0920-5861/$ – see front matter © 2008 Elsevier B.V. All rights reserved.
doi:10.1016/j.cattod.2008.06.029

out via solvent evaporation in a spin-coater followed by drying and surfactant removal under a residual pressure of 15 mbar as described in a previous work [16]. The WGS activity of the new catalyst was compared with that of pelletized gold catalysts supported on mesoporous titania via the deposition–precipitation method.

2. Experimental

2.1. Synthesis of Au/mesoTiO$_2$/TiO$_2$/Ti thin films

Titanium sheets (99.99 + wt.% Ti) of 9 mm length, 9 mm width, and with a thickness of 500 μm were used as substrates. Titanium samples were cleaned in boiling toluene for 1 h to remove organic contamination from the surface, dried in an oven at 413 K, and weighed. Generally, the surface of the titanium substrate is covered with a thin oxide layer [17]. The substrates were placed in a glass holder at a distance of ca. 0.5 mm from each other. They were then treated with a mixture (180 ml) of 4.3 vol.% H_2O_2 (Fluka) and 3.6 vol.% NH_4OH at 80 °C for 45 s, whereupon they were rinsed with demi-water and treated with 4 M NaOH solution at 60 °C for 30 s. The plates were rinsed again with demi-water and placed in an oven at 80 °C for 30 min before being oxidized at 60 °C for 6 h in a 30 vol.% aqueous H_2O_2 solution and calcined at 500 °C to remove peroxide species. Just before the synthesis, the titania layer was made super hydrophilic by an UV treatment for 2 h to provide a better adhesion of the titania film to the substrate. A detailed explanation of the cleaning procedures can be found elsewhere [18].

Colloidal gold nanoparticles of 4 nm diameter were synthesized following the polyol reduction method, as described previously [19], using gold (III) chloride hydrate (Aldrich) as the noble metal precursor. The only substantial difference between the approach described here and that available in the literature is that in this case, the nanoparticles were dispersed in absolute ethanol instead of dry methanol.

Nanoparticle-doped mesoporous titania thin films were prepared using a precursor solution of the following composition: 1 TiO_2 (titanium tetrabutoxide (TTB), Aldrich):0.005 Pluronic F127:40 EtOH:1.3 H_2O:0.13 HNO_3. The incorporation of Au nanoparticles was achieved using the ethanolic nanoparticle suspension to obtain a final 1 wt.% Au loading in mesoporous titania. The solution was then prepared by adding the appropriate amounts of F127, water, and TEOS, in that order. The bottle was then capped and the mixture stirred at room temperature for 2 h. An aliquot (50 μL) of the resulting sol was placed on the support and spin-coating was performed for 30 s at 1500 rpm with an acceleration rate of 1250 rpm/s. Drying and calcination were performed in an oven at a residual pressure of 15 mbar. The heating rate from 25 to 300 °C was 1 °C/min, with a 1 h dwelling time every 25 °C below 200 °C, a 2 h dwelling time at 225, 250 and 275 °C, and a 4 h dwelling time at 300 °C.

2.2. Thin film characterization

The morphology of the coatings was determined by transmission electron microscopy (TEM). High-resolution TEM studies were performed using a JEOL JEM-3011 electron microscope operating at 300 kV with a structural resolution of 0.16 nm. The average gold particle size, d_{av}, was calculated from the following formula: $d_{av} = \sum n_i d_i / \sum n_i$, where n_i is the number of particles of diameter d_i. Ellipsometric porosimetry (EP) was used to determine the mean pore size, pore size distribution and mesopore surface area. Prior to adsorption, the samples were treated under a residual pressure of 0.1 mbar at 300 °C for 30 min to remove all adsorbed species. The temperature was then decreased to 14 ± 0.2 °C and the ethanol (Merck, 99.99 wt.%) partial pressure was increased to saturation pressure. The lowest partial pressure of ethanol was 0.10 mbar and the saturation pressure, calculated by Antoine's equation, was 41 mbar. The pore volume and film thickness were determined from the change in the effective refractive index in the range 300–1200 nm. The thickness of the mesoporous titania layer was found to be 170 nm. The refractive index of the dry (ethanol-free) mesoporous film (n_M) and the total non-porous fraction (f_M) was calculated from the change in effective refractive index (n_{ef}) at the end points of the isotherm using the Bruggeman effective medium approximation (BEMA, Eq. (1)) and the refractive indeces of air and ethanol (n_m = 1.0 and 1.361 at 633 nm, respectively) [20].

$$f_M \frac{n_M^2 - n_{ef}^2}{n_M^2 + 2n_{ef}^2} + (1 - f_M) \frac{n_m^2 - n_{ef}^2}{n_m^2 + 2n_{ef}^2} = 0 \quad (1)$$

The effective refractive index as a function of the ethanol partial pressure (P/P_0), was measured using an ellipsometer. The isotherm was determined by fitting volumetric fractions of the inorganic component (f_M), ethanol (f_{ET}), and air with the BEMA at each relative pressure:

$$f_M \frac{n_M^2 - n_{ef}^2}{n_M^2 + 2n_{ef}^2} + f_{ET} \frac{1.361^2 - n_{ef}^2}{1.361^2 + 2n_{ef}^2} + (1 - f_{ET} - f_M) \frac{1.00 - n_{ef}^2}{1.00 + 2n_{ef}^2} = 0 \quad (2)$$

The ethanol volume adsorbed (V_{ET}) is related to the product of the total film volume (V_F), the pore fraction ($1 - f_M$), and the volumetric fraction of the ethanol saturated film (f_{ET}):

$$V_{ET} = V_F (1 - f_M) f_{ET} \quad (3)$$

The total mesoporous surface area was calculated from the average pore diameter, the total pore volume and the pore fraction assuming a cylindrical pore geometry.

X-ray diffraction analysis was performed on a Rigaku Geigerflex diffractometer using Cu Kα radiation (λ = 1.5405 Å, voltage 40 kV, and current 30 mA) with continuous scanning at a rate of 2° 2θ/min in the ranges of 1.5–6° and 20–90° 2θ. Long-order structure was not observed. In the wide angle part of the diffraction pattern there were four intense peaks, at 38.44°, 40.12°, 53.04° and 70.7° 2θ, corresponding to the titanium substrate. No peaks that can be assigned to crystalline phases of titania appeared in the XRD spectra. Moreover, XRD patterns did not reveal peaks related to gold, confirming that the gold was deposited as small nanoparticles.

2.3. Catalytic activity tests

The microstructured reactor has an AISI 316 stainless steel housing with standard tube connections and can be heated up to 350 °C with an electrical furnace. Details of the reactor geometry are given elsewhere [21]. The amount of heat released in the course of the reaction was always below 0.01 W. This is negligible as compared with the 10 W power load of the heating block. The heating block was made of a highly conductive material (78 W/(mK)) and was well insulated. The following estimation demonstrates that isothermal behavior of the reactor is to be expected. To avoid heat transfer limitations in the catalytic film, Mears criterion for heat transfer limitations of $-\Delta H_r r \rho t E / h T^2 R_g$ should be below 0.15, where ΔH_r is the enthalpy of the WGS reaction, r is the reaction rate, ρ is the apparent density of the catalytic film, t is the thickness of the film, E is the activation energy of the WGS reaction, h is the heat transfer coefficient, T is the temperature and R is the

ideal gas constant. This criterion was tested using the differential reactor data. The thermal Mears criterion always adopted values in the range between 10^{-3} and 10^{-4} and therefore there was no observation of a temperature gradient within the catalytic film.

To check for external mass transfer limitations in microchannels, the Mears criterion for laminar flow (Re = 4 in this study) was applied:

$$\frac{k_{rxn} d_t}{2k_g} < 0.1 \quad (4)$$

d_t stands here for the hydraulic diameter of the channel, r_{eff} for the effective rate of reaction, and k_g for the mass transfer coefficient. The mass transport coefficient k_g was found from the Sherwood number for fully developed laminar flow between two parallel plates to be 7.54. A maximum value of 0.003 was determined for Eq. (4), and thus no external mass transfer limitations are to be expected.

The activity tests were carried out at atmospheric pressure by changing the number of coated plates inserted in the microstructured reactor. To attain the required amounts of water vapour in the gas feed mixture, a helium flow was fed through a saturator, which was kept at a desired temperature. The overall flow rate was changed in the range of 30–50 ml/min (STP). The total coating volume was 0.03–0.15 cm^3 corresponding to a GHSV in the range 20,000–100,000 h^{-1}. The pressure drop over the microchannels was calculated to be less than 1 mbar. The use of a microstructured reactor makes kinetic analysis much simpler since the reactor can be operated in differential mode. To determine the reaction order of a compound its concentration needs to be varied while concentrations of the other components are kept constant. In this work, the total flow rate was kept constant by adjusting the He flow rate and to determine the CO reaction order, CO partial pressure was varied between 0.6 and 3.0 kPa at a constant water partial pressure of 15 kPa. To determine the H_2O reaction order, H_2O partial pressure was varied between 1.3 and 3 kPa at a constant CO pressure of 0.6 kPa. The temperature was measured by a thermocouple located at the centerline of the reactor. In these experiments, CO conversion was kept below 15%. The concentrations of the components in the effluent gas were analyzed using a Varian GC (CP-3800) equipped with TCD detectors. H_2 and CO were analyzed on a molecular sieve 5 Å column (0.25 mm ID, 10 m), and CO_2 and H_2O were analyzed on a poraPLOT-U column (0.25 mm ID, 10 m). The reaction rates were calculated from the product analysis using the differential reactor approximation. In all cases the rates were stable and reproducible. The pure TiO_2 coating was found to be inactive for the WGS reaction in the temperature region considered in this study.

3. Results and discussion

Determination of the pore structure of the deposited thin films is paramount for the development of the approach proposed in this study. Fig. 1 shows the ethanol adsorption isotherm at 14 °C for both a TiO_2 thin film and a Au-doped TiO_2 thin film achieved using the aforementioned technique. At low P/P_0 pressure, a steep rise in ethanol uptake, followed by a flat curve, corresponds to the filling of micropores with ethanol. The sharpness of the inflection in the ethanol isotherm on both Au/TiO_2 and TiO_2 films around P/P_0 = 0.3–0.5 indicated that the pores are in the mesoporous region and that their pore size distribution is narrow (Fig. 1). It can be seen that the shape of the adsorption isotherms did not change significantly. The typical type IV adsorption–desorption isotherm with a H_1 hysteresis loop and steep rises at low relative P/P_0 pressure indicate that both micro- and mesopores are present [22].

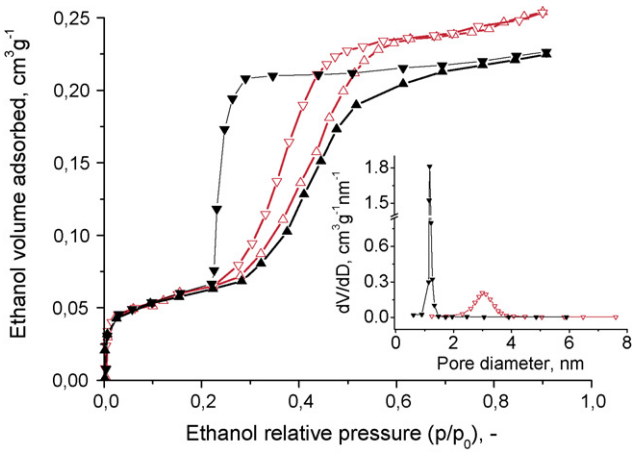

Fig. 1. Ethanol adsorption–desorption isotherms at 14 °C on Au/TiO_2 (solid symbols) and TiO_2 (hollow symbols) thin films and corresponding pore size distribution (inset).

Addition of 1 wt.% nanoparticles to the synthesis solution brings about a decrease in the mesopore surface area from 260 to 220 m^2/g and the mesopore volume from 0.18 to 0.15 cm^3/g as compared to that in the mesoporous titania film. The decrease in the mesopore volume suggests that Au nanoparticles are located inside the mesopores. Since the pore volume is only slightly changed, this decrease might be due to pore mouth blockage by Au nanoparticles, and as a result the ethanol desorption occurs via smaller pore openings or via the microporous network, and thus the hysteresis loop changes from being a H_1 to being a H_2 type. It should be noted that the micropore surface area cannot be evaluated by ellipsometric porosimetry.

TEM images of the films scratched off the titanium substrates (Fig. 2) revealed the open accessible structure of the mesostructured titania layer. The particle size distribution histogram (shown as an inset in Fig. 2) was obtained from a count of one hundred different nanoparticles. The TEM images indicated that the pore

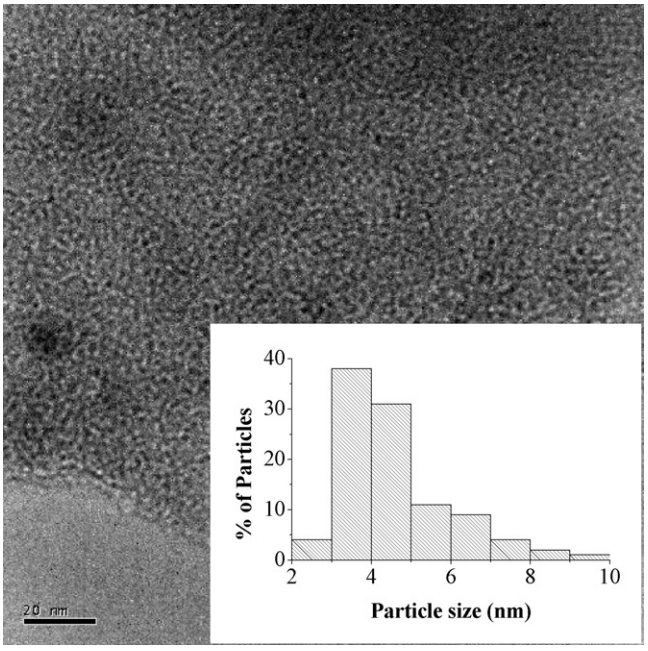

Fig. 2. TEM micrograph of mesoporous titania film and particle size distribution of the gold nanoparticles.

size of the deposited titania layer was slightly higher than 2 nm, which is substantially smaller than the average gold nanoparticle size. In principle, this would represent a problem should deposition of the colloids be sought after spin-coating of the titania thin film. In our case, however, confinement of the gold nanoparticles inside the inorganic matrix formed a mesoporous structure, with the nanoparticles constraining access to the porous cavities.

The catalytic activity of the gold supported on mesoporous titania thin films was investigated for the WGS reaction employing a CO/H_2O mixture in the 200–280 °C temperature range. No methanation products were observed. Fig. 3 shows the normalized short-term deactivation behavior of the coatings under real WGS conditions at 280 °C. The catalytic activity decreases by 15% over 2 days and, thereafter, remains rather constant. The absence of XRD peaks in the high angle region (not shown) demonstrates that the Au/TiO_2 films retain their amorphous structures after calcination at 300 °C. However, exposure of the titania films to the reaction mixture at 280 °C led to a partial collapse of mesoporous structure during the transformation from amorphous titania to anatase. This is inevitable at elevated temperatures and results in partial collapse of the mesopores [23]. As a result, Au nanoparticles can be rendered physically inaccessible by the inorganic network. This transformation took ca. 50 h on-stream time at 280 °C, after which no further deactivation was observed. At temperatures of 220 °C or less this phase transition was not observed and, therefore, in catalytic tests carried out at or below this temperature, catalysts maintained their initial activity levels.

It should be noted that the coatings were calcined at 300 °C under 15 mbar residual pressure to remove excess surfactant. The literature contains very little work on the WGS reaction where the effect of the calcination temperature on catalytic activity and stability of gold supported nanoparticles has been systematically studied. Hua et al. have shown that Au/iron oxide catalysts calcined either at 200 or 250 °C at atmospheric pressure showed the highest catalytic activity in the WGS reaction below 200 °C, and that this activity decreased with increasing calcination temperature [24]. For supported Au catalysts calcined at 300 °C and operating at reaction temperatures of below 225 °C, the activity varied depending on the support material as follows: $TiO_2 > CeO_2 \gg Al_2O_3$ [12]. In a different study [16], Au/TiO_2 catalysts calcined at 300 °C showed WGS catalytic activity which was from 1.5 to 2 times higher than that achieved using samples calcined either at 200 or 400 °C. An average reported gold particle size of 4 nm was similar to that applied in the present study. When calcined at 400 °C gold nanoparticles supported on TiO_2 [9,12,13] or TiO_2 nanotubes [25] showed high stability in a CO/H_2O mixture below 300 °C. However, it was not clearly justified why this temperature was chosen. Overall, it can be assumed, based on the results of our and other studies, that the calcination temperature should be 50–75 K higher than the highest reaction temperature to get stable catalysts.

To determine the reaction orders with respect to reactants, kinetic data were fitted to a power-rate law expression. Such an expression is very useful for the design of reactors. The experimentally determined reaction orders are presented in Fig. 4. To illustrate the quality of the kinetic data, the WGS reaction rate is plotted in double-logarithmic scale. The values for β ($\beta = [CO_2][H_2]/(K_p[CO][H_2O])$) in our experiments were usually of the order of 0.01–0.05, which indicates that the reaction was carried out far from equilibrium. High temperature data revealed that the reaction was first order with respect to CO. As the temperature is decreased, the reaction order with respect to CO slightly decreases, reaching 0.83 ± 0.05 at 220 °C. The order of the water reaction remains constant and rather low (0.10 ± 0.05) at the H_2O/CO ratios monitored. CO adsorption on Au nanoparticles is known to be weak [26,27], therefore the steady-state CO coverage is rather low under reaction conditions, and the increase in CO coverage induced by an increase of the CO partial pressure has a positive influence on the reaction rate. For water, the type of active metal does not seem to play an important role and different values between 0 and 0.5 are reported on different catalysts [10,11,28,29].

Some of the results published in the field over the last 2 years are compared with our data in Fig. 5. Comparison of reaction rates with those in the literature is complicated by the fact that most studies were carried out under different conditions and the inhibitory effect of CO_2 and H_2 on the WGS reaction rate was not studied explicitly. Not accounting for the effect of products (CO_2 and H_2) in a power-rate law expression results in the calculation of much higher rates compared to those achieved under the conditions prevalent after a reformer in fuel cell applications. We observed a more than two-fold decrease in the overall reaction rate when the CO/H_2O mixture was replaced by a simulated

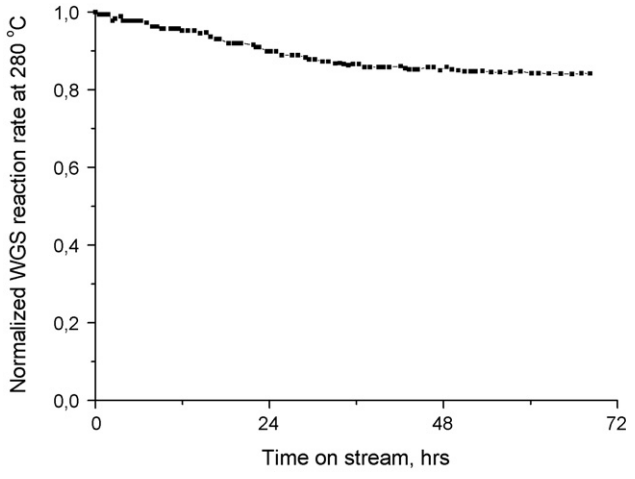

Fig. 3. Normalized short-term deactivation behavior of the Au/TiO_2 coatings at 280 °C in a mixture containing 3 vol.% CO, 15 vol.% H_2O, 3 vol.% CO_2, 55 vol.% H_2, balanced by He. Total flow was 50 ml/min (STP). The initial CO conversion was calculated as an average of the first two measurements obtained within an interval of 6 min.

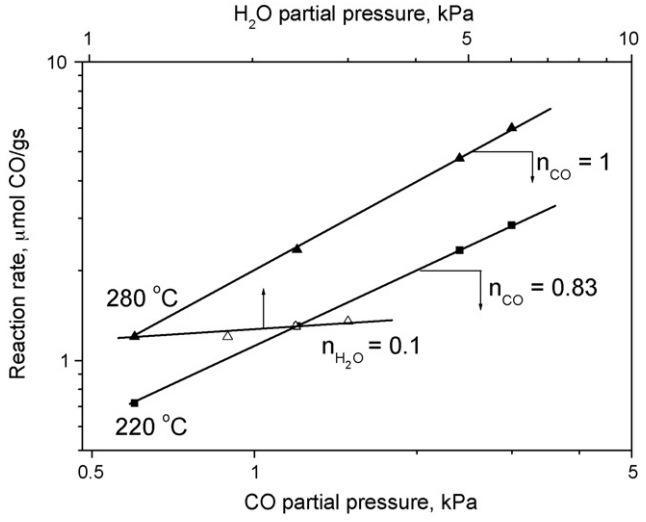

Fig. 4. Determination of power-rate law reactant reaction orders on the Au/TiO_2 thin films. The CO reaction order was determined at a constant water partial pressure of 15 kPa. The H_2O reaction order was determined at 280 °C and at a constant CO pressure of 0.6 kPa.

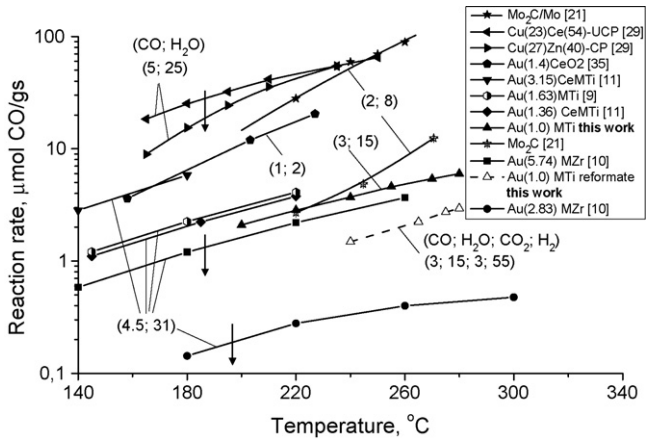

Fig. 5. Comparison of the WGS reaction rate on different catalytic systems with CO conversions lower than 20%. The data from Refs. [10,11,14] at the CO conversions of above 20% were plotted assuming that the reaction rate was first order in CO and that the catalyst bed showed plug-flow reactor behavior. The reactant volumetric fractions are given in parentheses. *Abbreviations*—CP: prepared by co-precipitation from nitrate salts by ammonium carbonate solution; UPC: prepared by homogeneous co-precipitation from nitrate precursors with urea in an ethylene glycol–water mixture; MTi: mesoporous titania; CeMTi: ceria modified mesoporous titania; MZr: mesoporous zirconia. The results where deactivation of catalysts has been reported are denoted "↓".

reformate gas (Fig. 5). It should be noted that the determination of kinetic constants using a CO/H_2O mixture gives values of rate constant that are lower than the actual ones and that this, in turn, results in the calculation of an activation energy that is lower than the actual one. For example, the apparent activation energy would be half of the actual value if the product of a reaction of order −1 was not included in the rate expression. Such anomalous behavior of activation energy values was reported for Cu–Ce–Zr catalysts [29] when the reactant mixture was replaced by the reformate one. In the present study, the apparent activation energy was increased from 28.6 to 40.8 kJ/mol by replacing the CO/H_2O mixture with the reformate gas. The former value is close to the 31 kJ/mol figure reported previously for an Au/TiO_2 catalyst in a CO/H_2O reactant mixture at 100 °C [12].

Keeping this in mind, we can compare the WGS rates normalized per unit of catalyst mass. Three classes of WGS catalyst are currently being developed: (i) Cu-containing bulk mixed metal oxide (MMO) catalysts [29,30]; (ii) noble metal deposited on mesoporous oxides [9–11]; (iii) molybdenum carbides (bulk deposited on metal substrates) [7,21,31,32]. A literature survey reveals that within any one class of catalyst, close values of reaction rate and apparent activation energy are observed under similar conditions. Both MMO and molybdenum carbide catalysts show higher activity in the WGS reaction when compared to supported gold catalysts. However, a high deactivation rate was reported on flame-sprayed MMO catalysts [29], where initial activity decreased by 10% after 10 h of exposure to the reformate mixture at 310 °C, independent from the feed conditions. In contrast to Au/TiO_2 coatings, no stabilization of the final catalyst was reported. This led the authors to suggest that the high surface area bulk catalysts have rather unstable surfaces that are prone to sintering. In the case of Mo_2C catalysts prepared by molten salt synthesis [21], deactivation was not observed. However, for these systems the ratio of coating to substrate thickness remains, at ca. 0.1, rather low, and this results in the need for a larger reactor size. In spite of this drawback, these catalysts can be applied above 300 °C, where they retain their high stability [21]. It should be noted that in our experiments CO partial pressure was 1.5 times lower than that used in Refs. [11,14]. Based on the observation of first order kinetics with respect to CO, one may calculate a WGS reaction rate of 4.3 μmol/(g s) at 220 °C, and this is comparable to rates of 4.1 and 3.8 μmol/(g s) reported by Idakiev et al. for Au (1.63 wt.%) supported on mesoporous titania [9] and Au (1.36 wt.%) supported on ceria modified mesoporous titania [11], respectively. Thus, the performance of Au/TiO_2 coatings appears not to be superior to pelletized catalysts with similar gold loadings in terms of activity and short-term stability. This is completely different to what has been observed for other thin film catalysts in different reactions, such as WGS [21] in which incorporation of the catalysts is performed after the thin film is deposited, hydrocarbon ammoxidation [18], and complete oxidation [33], where activities were reported that were between several times and an order of magnitude higher than that achieved using the corresponding pelletized catalysts in the absence of mass and heat transfer limitations. In particular, Mo_2C coatings deposited on a Mo substrate showed a remarkable increase in the WGS reaction rate as compared with the bulk Mo_2C phase (Fig. 5). We attributed this increase in catalytic activity to a strong thin film–substrate interaction effect which is similar to the well-known SMSI (strong metal support interaction) effect between the metal particles and their porous support. The absence of this "substrate effect" in case of gold supported titania thin films may be due to there being a weak interaction between the titania thin films and the Ti substrate owing to the production of a non-porous titania "barrier" during oxidation in the H_2O_2 solution prior to the coating synthesis.

Compared to both the commercial $Cu/ZnO/Al_2O_3$ and Au/CeO_2 WGS catalysts, Au/TiO_2 catalysts reveal rather small activation barriers. Thus, this catalyst can be applied over a larger temperature range. Furthermore, activation energies 15–20 kJ/mol higher have also been reported for other Ce- and Mo-containing catalysts under comparable reaction conditions [34]. For a typical reformate mixture composed of 3 vol.% CO, 13.5 vol.% CO_2, 27 vol.% H_2O, 56.5 vol.% H_2O [21], equilibrium is reached at ca. 300 °C, indicating that it is important to develop active coatings for the 180–250 °C temperature range (Fig. 6). Fig. 6 shows the WGS activity in the high conversion range as a function of reaction temperature at different GHSV. The Au (1 wt.%)/TiO_2 coatings showed CO conversion similar to that revealed by Mo_2C/Mo coatings at 220 °C, when the contact time was decreased by a factor

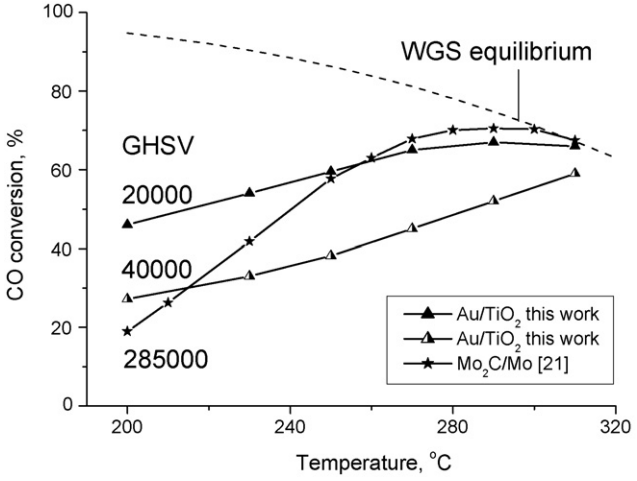

Fig. 6. CO conversion as a function of reaction temperature for the Au/TiO_2 thin films compared to reference Mo_2C/Mo thin films with the best performance in the WGS reaction [21]. Gas composition: $p_{CO} = 3.0$ kPa, $p_{H_2O} = 15.0$ kPa, $p_{CO_2} = 13.5$ kPa and $p_{H_2} = 56.5$ kPa.

of 7. In agreement with the data obtained in the kinetic study, the high CO conversion temperature range is much wider for the Au/TiO_2 coatings. The shape of the conversion plot demonstrates that there are no external mass transfer limitations in the microreactor even at a high GHSV of 40,000 h^{-1}. It should be noted that the thickness of the Au/TiO_2 thin films can be increased considerably by repetition of spin-coating/drying steps. The maximum layer thickness to avoid internal mass transfer limitations can be estimated from the following equation:

$$\frac{R_{rxn}t^2}{D_{e\text{-}CO}C_{CO}}\frac{m+1}{2} < 0.1 \quad (5)$$

where R_{rxn} is volumetric reaction rate, C_{CO} is the CO concentration, m is the reaction order, $D_{e\text{-}CO}$ is the effective diffusivity of CO in the catalytic coating of 5.0×10^{-6} m^2/s, and t is the coating thickness. This results in a maximum layer thickness of ca. 330 μm. Thus, comparing WGS reaction rates per volume of microreactor rather than per coating weight, it is clear that rates beyond the state-of-the art value of 0.7 mol CO/m^3 s obtained with Mo_2C coatings [21], can be achieved.

4. Conclusions

Supported Au/mesoporous TiO_2 thin films with well-defined pore size prepared via a modified evaporation-induced self assembly process have been shown to be highly active for the WGS reaction in an idealized reaction gas mixture and also to be remarkably stable after an initial period, with an exponential deactivation by about 15% of the initial activity noted over 2 days. Ethanol adsorption–desorption isotherms showed that the Au nanoparticles were incorporated into a mesoporous titania network. A reaction order with respect to CO of 0.8–1.0 was determined on the 1.0 wt.% Au coating in the idealized WGS mixture. An activation energy of 28.6 kJ mol^{-1} was obtained in the temperature range 220–280 °C and this value was less affected by addition of CO_2 and H_2 in the feed as compared to activation barriers for Cu-based catalysts. The reaction rate measured at CO conversions of below 10% was similar to that reported for gold supported on mesoporous titania and for ceria modified mesoporous titania pelletized catalysts with similar gold loading and particle sizes.

Acknowledgements

The financial support by the Netherlands Organization for Scientific Research (NWO), project no. 047.017.029 and British Council–NWO Partnership Programme in Science, projects PPS 888 and 894, is gratefully acknowledged.

References

[1] J.M. Sohn, Y. Chang Byun, J. Yeon Cho, J. Choe, K. Ho Song, Int. J. Hydrogen Energy 32 (2007) 5103.
[2] B.J. Bowers, J.L. Zhao, M. Ruffo, R. Khan, D. Dattatraya, N. Dushman, J.C. Beziat, F. Boudjemaa, Int. J. Hydrogen Energy 32 (2007) 1437.
[3] D. Sopena, A. Melgar, Y. Briceno, R.M. Navarro, M.C. Alvarez-Galvan, F. Rosa, Int. J. Hydrogen Energy 32 (2007) 1429.
[4] G. Kolb, J. Schurer, D. Tiemann, M. Wichert, R. Zapf, V. Hessel, H. Lowe, J. Power Sources 171 (2007) 198.
[5] W. Ehrfeld, V. Hessel, H. Lowe, Microreactors, Wiley–VCH, Weinheim, 2003.
[6] T.S. Glazneva, E.V. Rebrov, J.C. Schouten, E.A. Paukshtis, Z.R. Ismagilov, Thin Solid Films 515 (2007) 6391.
[7] S.A. Kuznetsov, A.R. Dubrovskiy, E.V. Rebrov, J.C. Schouten, Z. Naturforsch. 62a (2007) 647.
[8] A. Kuperman, M.E. Moir, Method for making hydrogen using a gold containing water-gas shift catalyst, US Patent 7,169,376 (2007).
[9] V. Idakiev, T. Tabakova, Z.-Y. Yuan, B.-L. Su, Appl. Catal. A. 270 (2004) 135.
[10] V. Idakiev, T. Tabakova, A. Naydenov, Z.-Y. Yuan, B.-L. Su, Appl. Catal. B 63 (2006) 178.
[11] V. Idakiev, T. Tabakova, K. Tenchev, Z.-Y. Yuan, T.-Z. Ren, B.-L. Su, Catal. Today 128 (2007) 223.
[12] H. Sakurai, A. Ueda, T. Kobayashi, M. Haruta, Chem. Commun. 3 (1997) 271.
[13] F. Boccuzzi, A. Chiorino, M. Manzoli, D. Andreeva, T. Tabakova, L. Ilieva, V. Idakiev, Catal. Today 75 (2002) 169.
[14] P. Panagiotopoulou, A. Christodoulakis, D.I. Kondarides, S. Boghosian, J. Catal. 240 (2006) 114.
[15] A. Sandoval, A. Gómez-Cortés, R. Zanella, G. Díaz, J.M. Saniger, J. Mol. Catal. A 278 (2007) 200.
[16] O. Muraza, E.V. Rebrov, T. Khimyak, B.F.G. Johnson, P.J. Kooyman, U. Lafont, M.H.J.M. de Croon, J.C. Schouten, Chem. Eng. J. 135 (2008) S99.
[17] R.L.P. Teixeira, G.C.D. de Godoy, M. de M. Pereira, Mater. Res. 7 (2004) 299–303. , doi:10.1590/S1516-14392004000200013 [online].
[18] M.J.M. Mies, E.V. Rebrov, J.C. Jansen, M.H.J.M. de Croon, J.C. Schouten, J. Catal. 247 (2007) 328.
[19] S. Dominguez-Dominguez, A. Berenguer-Murcia, D. Cazorla-Amoros, A. Linares-Solano, J. Catal. 243 (2006) 74.
[20] V.A. Tomalchev, J. Opt. Technol. 68 (2001) 328.
[21] E.V. Rebrov, S.A. Kuznetsov, M.H.J.M. de Croon, J.C. Schouten, Catal. Today 125 (2007) 88.
[22] S.J. Gregg, K.S. Sing, Adsorption, Surface Area and Porosity, Academic Press, New York, 1982.
[23] D. Grosso, G.J. de A.A. Soler-Illia, F. Babonneau, C. Sanchez, P.-A. Albouy, A. Brunet-Bruneau, A.R. Balkenade, Adv. Mater. 13 (2001) 1085.
[24] J. Hua, K. Wei, Q. Zheng, X. Lin, Appl. Catal. A 259 (2004) 121.
[25] V. Idakiev, Z.Y. Yuan, T. Tabakova, B.L. Su, Appl. Catal. A 281 (2005) 149.
[26] S. Derrouiche, P. Gravejat, D. Bianchi, J. Am. Chem. Soc. 126 (2004) 13010.
[27] D.C. Meier, D.W. Goodman, J. Am. Chem. Soc. 126 (2004) 1892.
[28] S. Hilaire, X. Wang, T. Luo, R.J. Gorte, J. Wagner, Appl. Catal. A 215 (2001) 271.
[29] F. Huber, H. Meland, M. Ronning, H. Venvik, A. Holmen, Top. Catal. 45 (2007) 101.
[30] F. Huber, Z. Yu, J.C. Walmsley, D. Chen, H.J. Venvik, A. Holmen, Appl. Catal. B 71 (2007) 7.
[31] M. Nagai, K. Matsuda, J. Catal. 238 (2006) 489.
[32] M. Nagai, A.Md. Zahidul, K. Matsuda, Appl. Catal. A 313 (2006) 137.
[33] I.Z. Ismagilov, R.P. Ekatpure, L.T. Tsykoza, E.V. Matus, E.V. Rebrov, M.H.J.M. de Croon, M.A. Kerzhentsev, J.C. Schouten, Catal. Today 105 (2005) 516.
[34] R. Leppelt, B. Schumacher, V. Plzak, M. Kinne, R.J. Behm, J. Catal. 244 (2006) 137.